

PACS numbers: 42.25.Ja; 42.25.Lc; 42.79.Fm
DOI: 10.1070/QE2006v036n05ABEH013247

Polarisation splitting of laser beams by large angles with minimal reflection losses

B.L. Davydov

***Abstract*. New crystal anisotropic prisms for splitting orthogonally polarised components of laser radiation by large angles with minimal reflection losses caused by the Brewster refraction and total internal reflection of polarised waves from the crystal – air interface are considered and the method for their calculation is described. It is shown that, by assembling glue-free combinations of two or three prisms, thermally stable beamsplitters can be fabricated, which are free from the beam astigmatism and the wave dispersion of the output angles of the beams. The parameters and properties of new beamsplitters are presented in a convenient form in figures and tables.**

Keywords: *polarisers, polarisation beamsplitters, laser equipment components.*

1. Introduction

Polarisation beamsplitters based on anisotropic crystals are well known in optics. These are composite Nicol, Thompson, Glan, Wollaston, Rochon, Senarmont and other prisms [1]. They consist of prisms connected either with transparent glue or via the air gap. The angular splitting of polarised beams occurs at the interface of the prism components. Modern lasers producing light beams with powers of tens and hundreds watts impose strict requirements to the radiation resistance of these devices. In these cases, prisms with air gaps are used in which a light beam propagating through the prism intersects the air gap at the non-Brewster angle, partially reflecting from two surfaces. The reflection losses can amount to 5 % and more. Such high reflections are undesirable at intense light fluxes because they correspond to such high absolute powers that the problem of their safe utilisation appears, to say nothing of a high cost of each lost watt of laser radiation.

In this paper, we describe the method for polarisation splitting of laser beams with minimal reflection losses, which is based on the simultaneous realisation of non-dissipative processes of the total internal reflection (TIR) of the ordinary (o) wave and refraction of the extraordinary (e) wave strictly at the Brewster angle on one of the crystal faces [2]. This method provides the spatial separation of orthogonally polarised waves by tens of degrees, and the corresponding prisms can be used with light beams of large diameters, unlike polarisation prisms for small-diameter beams [3].

B.L. Davydov Institute of Radio Engineering and Electronics, Russian Academy of Sciences, pl. akad. Vvedenskogo 1, 141120 Fryazino, Moscow region, Russia; e-mail: bld_res2000@rambler.ru, bld_res2001@pocta.ru

Received 13 December 2005
Kvantovaya Elektronika **36** (5) 473 – 482 (2006)
Translated by M.N. Sapozhnikov

2. Splitting of the o- and e-waves with minimal reflection losses

We will find criteria for the splitting of orthogonally polarised waves in uniaxial crystals which are mainly used in polarisation optics. As for biaxial crystals, the expressions presented below are also valid for them for light beams propagating in one of the principal planes of the optical indicatrix.

Thus, we consider the general case of noncollinear orthogonally polarised waves produced after the TIR of a nonpolarised beam from one of the crystal faces. Figure 1 shows the section of a rectangular prism in which this can be realised. In this section, which is parallel to the prism base, the wave vectors of the propagating waves are shown. Because the lateral faces in the prism are perpendicular to bases, we will denote these faces by the section boundaries. Let a nonpolarised wave with the wave vector $\boldsymbol{K}_{\rm in}$ be incident normally from an external isotropic medium on the transparent face AB of the crystal, whose optical axis is located in the plane of incidence. The o- and e-waves experience TIR on the AB face, after which their wave vectors prove to be noncollinear, with the angle δ between them. Let us require that the p-polarised wave (here, the e-wave) would refract at the Brewster angle on the next BC face, while the o-wave would experience TIR from this face. It follows from the FGH triangle in Fig. 1 that the criterion for the fulfilment of this requirement has the form

$$|\delta| \geqslant \delta_{\rm cr} = \arcsin\frac{1}{n_{\rm o}} - \alpha_{\rm in}^{\rm Br}, \qquad (1)$$

where $\delta_{\rm cr}$ is the critical (minimal) splitting angle of polarised waves; $\alpha_{\rm in}^{\rm Br}$ and its conjugate angle $\alpha_{\rm out}^{\rm Br}$ are the internal and external Brewster angles calculated by formulas modified for the uniaxial crystal – isotropic medium interface [3]; and $n_{\rm o}$ is one of the two principal ($n_{\rm o}$ and $n_{\rm e}$) refractive indices.

Before proceeding to the analysis of expression (1), we consider for generality a simpler particular case of collinear o- and e-waves, when $\delta = 0$. The latter is possible for the angle of incidence $\alpha = 0$, i.e., when the AB face is made

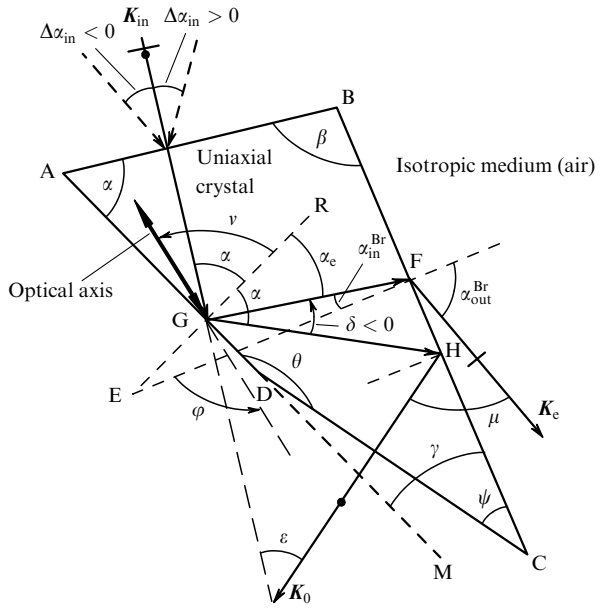

Figure 1. Orthogonally polarised waves in a uniaxial crystal prism.

coincident with the AD face. A nonpolarised wave enters the crystal normally through the AD face and then propagates in it without TIR in the form of two collinear o- and e-waves. In crystal optics, two types of orientation of the optical axis are most frequently used: the axis is either perpendicular to the plane of incidence or lies in this plane. Let us find for both these orientations the criteria for simultaneous existence of TIR and Brewster refraction for collinear waves on a common crystal face. Because in the case of the first orientation, the p-polarised wave is the o-wave, the required criterion is obvious:

$$\arctan \frac{1}{n_o} \geqslant \arcsin \frac{1}{n_e}, \tag{2a}$$

or

$$(n_e - n_o) \geqslant (n_e + n_o)^{-1}. \tag{2b}$$

Note that for the first orientation of the optical axis in a uniaxial crystal, the variant of noncollinear o- and e-waves obtained upon TIR in a plane perpendicular to the axis is impossible.

For the second orientation of the optical axis, the p-polarised wave is the e-wave, and the corresponding criterion follows directly from (1) for $\delta = 0$:

$$\alpha_{in}^{Br} \geqslant \arcsin \frac{1}{n_o}, \tag{3a}$$

or

$$(n_o - n^*) \geqslant (n_o + n^*)^{-1}. \tag{3b}$$

Here, n^* is the number formally defined by the expression $n^* = 1/\tan \alpha_{in}^{Br}$.

Unlike isotropic media, this number in anisotropic media is not the refractive coefficient of the e-wave in the direction of the angle of incidence α_{in}^{Br}. It is obvious that to fulfil criteria (2a)–(3b), crystals with a high birefringence $\Delta n = |n_o - n_e|$ and large refractive indices n_o and n_e should be chosen.

Criterion (2a), (2b) can be fulfilled only in positive crystals, where $n_o > n_e$. Actually, only a TiO_2 rutile crystal of all the crystals used in polarisation optics satisfies this criterion. However, so far the application of high-quality rutile crystals of a large size is considerably restricted by their high cost.

Criterion (3a), (3b) can be fulfilled in negative crystals, where $n_e > n_o$. However, by calculating from expressions in [3] the values of n^* for the main negative crystals used in polarisation optics such as $CaCO_3$, α-BaB_2O_4 (α-BBO), $LiIO_3$ [*], and $LiNbO_3$, we see that criterion (3a), (3b) is not fulfilled in them with a large 'margin' for any angles φ (Fig. 1). This means that it is impossible to fabricate from these crystals a prism with a face on which collinear polarised beams could be split upon TIR and exact Brewster refraction.

The situation changes basically upon noncollinear incidence of waves on the interface of media. In this case, condition (1) can be satisfied in many positive and negative crystals having even small values of Δn. Let us consider again Fig. 1 and study the dependence of the angle δ between the wave vectors of the o- and e-waves on the orientation angle v of the optical axis with respect to the normal EGR and the angle of incidence α of the input wave on the AD face. By convention we assume that $\delta < 0$ if the angle of reflection of the e-wave from this face is smaller than the angle of reflection of the o-wave from the same face. The Snell equation for the reflection of the e-wave from the AGD face has the form

$$n_o n_e \sin\alpha \left[n_o^2 \sin^2(v-\alpha) + n_e^2 \cos^2(v-\alpha)\right]^{-1/2} \tag{4}$$

$$= n_o n_e \sin(\alpha+\delta) \left[n_o^2 \sin^2(v+\alpha+\delta) + n_e^2 \cos^2(v+\alpha+\delta)\right]^{-1/2}.$$

The analytic solution of this equation is

$$\delta = \alpha_e - \alpha, \tag{5}$$

where

$$\alpha_e = \arctan\left\{0.5b^{-1}\left[\left(c^2 + 4bd\right)^{1/2} - c\right]\right\};$$

$$b = 1 - a\left[\sin^2 v + \left(\frac{n_o}{n_e}\right)^2 \cos^2 v\right];$$

$$c = a\left[1 - \left(\frac{n_o}{n_e}\right)^2\right] \sin 2v;$$

$$d = a\left[\cos^2 v + \left(\frac{n_o}{n_e}\right)^2 \sin^2 v\right];$$

$$a = \sin^2\alpha \left[\left(\frac{n_o}{n_e}\right)^2 \sin^2(v-\alpha) + \cos^2(v-\alpha)\right]^{-1}.$$

Let us analyse solution (5) by the example of a $CaCO_3$ crystal ($n_o = 1.6425$, $n_e = 1.4797$) for radiation at 1.064 μm. Figure 2 shows the function $\delta = F(\alpha, v)|_{\alpha=\text{const}}$ for angles

[*] Optically active crystal; polarisation ellipticity due to optical activity was neglected in calculations of prisms made of this crystal.

$\alpha = 45^\circ$ and 60°. The function has unequal extrema of opposite signs at the orientation angles of the optical axis $v_{\max} = 42^\circ$ and $v_{\min} = 138^\circ$, which are inherent only in this crystal. According to Fig. 1, condition (1) can be fulfilled only on the negative branches of this function [the minimum of the function $F(v)$ for positive crystals is located in the region $0 < v < 90^\circ$]. Let us recalculate functions $\delta = F(\alpha, v)|_{\alpha=\text{const}}$ to functions $\delta = F(\alpha, v)|_{v=\text{const}}$ for the angles $v = v_{\max}$ and $v = v_{\min}$. The moduli of these new functions are shown in Fig. 3. Note that the angle δ increases almost linearly with increasing the angle of incidence α. Let us find now the critical minimal angle δ_{cr} for the absolute value $|\delta|$. For this purpose, we calculate the angle φ between the optical axis and the normal EF, which is oriented so that the e-wave is refracted on the BFHC face at the Brewster angle. In this case, the Snell equation has the form

$$\sin\alpha_{\text{out}}^{\text{Br}} = n_{\text{o}} n_{\text{e}} \left[n_{\text{o}}^2 \sin^2(v + \alpha + \delta) + n_{\text{e}}^2 \cos^2(v + \alpha + \delta) \right]^{-1/2} \sin(\alpha + \delta + v - \varphi), \qquad (6)$$

where $\alpha_{\text{out}}^{\text{Br}}$ is the known function of the same angle φ [3]. This equation has the exact solution giving two values of φ for the two possible orientations of the BFHC face with respect to the optical axis. The first value corresponds to the propagation of the e-wave in air along the incident wave, while the second one corresponds to the propagation of this wave in the opposite direction. We are interested in the first value of φ, which is calculated from the expression

$$\varphi = -\arctan\left\{0.5q^{-1}\left[\left(t^2 - 4qr\right)^{1/2} + t\right]\right\} \qquad (7)$$

for positive crystals, and from the expression,

$$\varphi = \pi - \arctan\left\{0.5q^{-1}\left[\left(t^2 - 4qr\right)^{1/2} + t\right]\right\} \qquad (8)$$

for negative crystals, where

$$q = n_{\text{o}}^2\left(1 - n_{\text{e}}^2\right) - \left(1 - n_{\text{o}}^2 n_{\text{e}}^2\right) n_{\text{oe}}^2 \cos^2(v + \alpha_{\text{e}});$$

$$r = n_{\text{e}}^2\left(1 - n_{\text{o}}^2\right) - \left(1 - n_{\text{o}}^2 n_{\text{e}}^2\right) n_{\text{oe}}^2 \sin^2(v + \alpha_{\text{e}});$$

$$t = \left(1 - n_{\text{o}}^2 n_{\text{e}}^2\right) n_{\text{oe}}^2 \sin(2v + 2\alpha_{\text{e}});$$

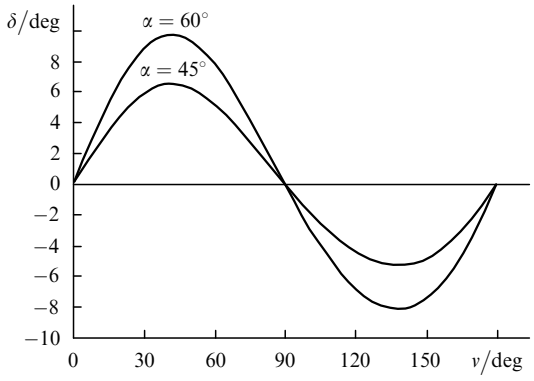

Figure 2. Splitting angle $\delta = F(\alpha, v)|_{\alpha=\text{const}}$ of polarised waves in a calcite crystal as a function of the orientation angle v of the optical axis and the angle of incidence α.

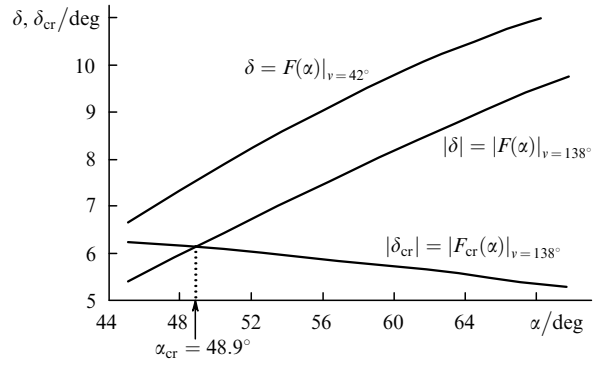

Figure 3. Determination of the critical angles of incidence α_{cr} and splitting δ_{cr} for the o- and e-waves in a calcite crystal.

$$n_{\text{oe}} = n_{\text{o}} n_{\text{e}} \left[n_{\text{o}}^2 \sin^2(v + \alpha_{\text{e}}) + n_{\text{e}}^2 \cos^2(v + \alpha_{\text{e}}) \right]^{-1/2}.$$

Now, knowing the angles φ, $\alpha_{\text{out}}^{\text{Br}}$, and $\alpha_{\text{in}}^{\text{Br}}$, we can calculate the function $\delta_{\text{cr}} = F_{\text{cr}}(\alpha)|_{v=138^\circ}$ from (1). Figure 3 shows the plot of the absolute value of this function. The intersection of the curves $|\delta_{\text{cr}}| = |F_{\text{cr}}(\alpha)|_{v=138^\circ}$ and $|\delta| = |F(\alpha)|_{v=138^\circ}$ gives the required critical angles $\delta_{\text{cr}} = 6.1^\circ$ and $\alpha_{\text{cr}} = 48.9^\circ$. Thus, if a prism is made of calcite with the orientation angle of the optical axis $v = 138^\circ$, the angle α between the input face and the first TIR face should exceed 48.9°. The larger is the angle α, the wider is the angular field of view of the prism, which depends on the angular 'margin' $\Delta\delta = \delta - \delta_{\text{cr}}$. However, because the prism size increases with increasing this angle, one should agree to a compromise in the selection of α.

In the next section, we present the results of calculations of the characteristic variants of prisms consisting of six basic crystals used in polarisation optics (expressions for the calculation of refractive indices of these crystals are presented below in Table 10). The particular angles δ and α were selected taking into account the preliminary calculated values of δ_{cr} and α_{cr} presented in Table 1.

Table 1.

Crystal	$v = v_{\min}$/deg	α_{cr}/deg	δ_{cr}/deg
$CaCO_3$	138	48.9	6.1
α-BBO	137.5	53.1	5.8
$LiIO_3$	137	45.8	4.3
$LiNbO_3$	136	53	2.5
YVO_4	48	48.7	5.9
TiO_2	48	36.6	3.7

3. Single-prism polarisation beamsplitters

The choice of the design of a polarisation prism beamsplitter follows from the propagation pattern of the o- and e-waves (Fig. 1). The first face AB is normal to the incident input beam. The second face AD is specified by the chosen angle α. The third face BC is determined by the calculated angle φ. The fourth face DC is normal to the output o-wave (it is assumed that all the faces normal to the light beams are polished and have AR coatings). As a result, the beamsplitter has the form of a rectangular prism with oblique-angled ABCD bases with the angle characteristics

$$\gamma = \alpha + \delta - \alpha_{\text{in}}^{\text{Br}},\ \beta = \pi - \alpha - \gamma,\ \psi = \alpha - \gamma,$$
$$\mu = \pi - \alpha_{\text{out}}^{\text{Br}} - \psi,\ \theta = \pi - \alpha + 2\gamma,\ \varepsilon = 2\gamma. \tag{9}$$

The field of view $\pm\Delta\alpha_{\text{in}}$ of the prism is limited either by the violation of TIR of the o-wave on the BC face or the admissible reflection of the e-wave upon deviations of its angle of incidence from the exact Brewster angle, or by both these factors. In this paper, we assume that the admissible reflection coefficient is $R_{\text{e}}^{\max} = 1\,\%$, which is calculated from the Fresnel formula modified for uniaxial crystals [3] or by the method considered in [4].

To determine the field of view and size of the prism, it is necessary to calculate the paths of the extreme rays in the input-beam cross section. The minimal size of the prism is determined by the absence of the light-beam vignetting on prism faces over the entire field of vision. The geometrical calculation for the o-waves and o-rays is elementary due to their collinearity. For the e-waves and e-rays, the walk-off angles of energy should be additionally calculated after each refraction (or reflection) event [3].

If the obtuse angle θ is expanded up to 180°, the four-face prism (i.e., a prism with four working lateral faces, which is denoted by the figure IV) transforms to a simpler trihedral prism (denoted by the figure III) in which the normal output of the o-wave through the AM face is possible only under the additional condition

$$\alpha = 2\gamma. \tag{10}$$

These two types of prisms with removed parts unfilled by light are show in Fig. 4. The angular and minimised linear parameters of the prisms are presented in Tables 2 and 3 (the notation corresponds to Fig. 1) and Tables 4–7 (the notation corresponds to Fig. 4). The calculations were performed for a 1.064-μm light beam of diameter $d_{\text{in}} = 5$ mm. To compare the sizes and angles, we present the angles α for each of the prisms. The prism parameters close to optimal values are shown in bold. Apart from the basic dimensions of the prisms, Tables 4–7 also present the

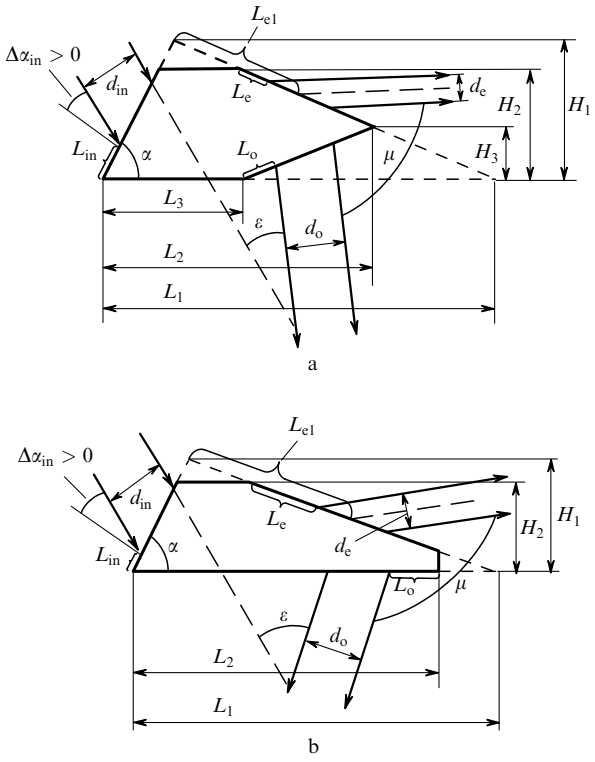

Figure 4. Angular and linear characteristics of prisms IV (a) and III (b).

Table 2.

Negative crystal	Prism type	α/deg	β/deg	γ/deg	ν/deg	ψ/deg	θ/deg	$\alpha_{\text{out}}^{\text{Br}}$/deg	μ^*/deg	ε^*/deg	$\Delta\alpha_{\text{in}}$/deg
$CaCO_3$	III	76.94	64.59	38.47	112	38.47	180	58.85	82.68	76.94	$+1.5^{**}$, -4.0^{***}
	IV	**60**	**99.96**	**20.04**	**138**	**39.96**	**160.08**	**59.55**	**80.49**	**40.08**	$+\mathbf{4.0}^{**}$, $-\mathbf{4.2}^{***}$
α-BBO	III	76.90	64.65	38.45	117.60	38.45	180	59.45	82.11	76.90	$+2.2^{**}$, -3.8^{**}
	IV	**64.6**	**90**	**25.39**	**137.50**	**39.21**	**166.18**	**59.87**	**80.94**	**50.78**	$+\mathbf{3.5}^{**}$, $-\mathbf{4.0}^{***}$
$LiIO_3$	III	**68.04**	**77.95**	**34.02**	**117**	**34.02**	**180**	**61.66**	**84.31**	**68.04**	$+\mathbf{2.6}^{**}$, $-\mathbf{3.0}^{***}$
	IV	62.63	90	27.36	137	35.26	172.11	62.28	82.46	54.73	$+4.9^{**}$, -3.0^{***}
$LiNbO_3$	III	53.27	100.1	26.63	136	26.63	180	65.96	87.41	53.27	$+0.04^{**}$, -2.0^{***}
	IV	65.38	76.70	37.92	136	27.46	190.46	66.05	86.49	75.84	$+1.8^{**}$, -2.0^{***}
	IV → III	**65.38**	**76.70**	**37.92**	**136**	**37.92**	**180**	**66.05**	**99.94**	**89.29**	$+\mathbf{1.8}^{**}$, $-\mathbf{2.0}^{***}$

* For normally incident input wave. ** Restriction due to frustrated TIR of the o-wave on the AB face. *** Restriction in the reflection level of the e-wave $R = 1\,\%$ on the AB face.

Table 3.

Positive crystal	Prism type	α/deg	β/deg	γ/deg	ν/deg	ψ/deg	θ/deg	$\alpha_{\text{out}}^{\text{Br}}$/deg	μ^*/deg	ε^*/deg	$\Delta\alpha_{\text{in}}$/deg
YVO_4	III	**64**	**84**	**32**	**30.4**	**32**	**180**	**65.06**	**82.93**	**64**	$+\mathbf{2.4}^{**}$, $-\mathbf{2.2}^{***}$
	IV	61.6	90.02	28.38	48	33.22	175.17	65.67	81.11	56.77	$+3.6^{***}$, -2.2^{***}
TiO_2	III	**53.81**	**99.28**	**26.91**	**48**	**26.91**	**180**	**70.1**	**83.02**	**53.81**	$+\mathbf{2.2}^{***}$, $-\mathbf{1.4}^{***}$
	IV	45	115.26	19.74	48	25.26	174.47	69.89	84.85	39.47	$+2.2^{***}$, -1.4^{***}

* For normally incident input wave; ** Restriction due to frustrated TIR of the o-wave on the AB face. *** Restriction in the reflection level of the e-wave $R = 1\,\%$ on the AB face.

coordinates L_{in}, L_e, and L_o of the boundaries of light beams on faces for the normal incidence of the input beam and for the edges of the field of view, as well as the relative angles μ and ε of the output beams only for the edges of the field of view (these angles for the normal incidence of light are presented in Tables 2 and 3). The e-beam going out to air is narrowed down in the plane of refraction, which is demonstrated by the ratio d_e/d_{in} of the beam diameters at input and output.

Our calculations showed that prisms III made of $CaCO_3$, α-BBO, and $LiIO_3$ crystals can be fabricated only with angles $v \neq v_{min}$ because for $v = v_{min}$ the angles of incidence satisfying the additional 'trihedral' condition (10) do not exist.

On the contrary, trihedral prisms made of positive yttrium vanadate YVO_4 and rutile TiO_2 crystals can be fabricated both with angles $v = v_{min}$ and $v \neq v_{min}$. The choice of a specific angle v depends sometime on the requirements imposed on the prism. For example, prism III made of the YVO_4 crystal can be calculated both with the 'convenient' angle $v_{min} = 48^\circ$ (with minimal requirements to the accuracy of the optical-axis orientation) and the 'inconvenient' angle $v = 30.4^\circ$, but in the latter case the prism proves to be shorter almost by one fourth. As a result, the choice of this angle should be determined by the user.

Calculations of many variants of prisms showed that the $LiIO_3$, YVO_4, and TiO_2 crystals are most suitable for fabricating prisms III of the minimal size, while the $CaCO_3$

Table 4.

Crystal	Prism type	α/deg	L_1/mm	L_2/mm	L_3/mm	H_1/mm	H_2/mm	H_3/mm	d_e/d_{in} $(+\Delta\alpha_{in})$	d_e/d_{in} $(\Delta\alpha_{in}=0)$	d_e/d_{in} $(-\Delta\alpha_{in})$
$CaCO_3$	III	76.94	27.16	27.16	–	18.22	6.97	–	0.67	0.63	0.52
	IV	**60**	**24.83**	**17.87**	**10.87**	**7.48**	**6.22**	**2.54**	**0.76**	**0.68**	**0.55**
α-BBO	III	76.9	26.70	26.70	–	17.89	6.75	–	0.68	0.63	0.52
	IV	**64.6**	**24.27**	**20.36**	**12.82**	**9.40**	**6.62**	**1.85**	**0.73**	**0.66**	**0.53**
$LiIO_3$	III	**68.04**	**14.39**	**14.39**	–	**7.64**	**4.64**	–	**0.63**	**0.57**	**0.46**
	IV	62.63	23.10	20.65	11.50	9.43	6.85	1.27	0.70	0.58	0.48
$LiNbO_3$	III	53.27	11.00	9.60	–	4.02	4.02	–	0.47	0.46	0.38
	IV → III	**65.38**	**12.43**	**12.43**	–	**7.14**	**4.55**	–	**0.52**	**0.46**	**0.38**

Notes: Displacement of the input beam in all prisms is $L_{in} = 0$; $d_o/d_{in} = 1$ in all prisms except prism IV → III; in prism IV → III, $d_o/d_{in} = 0.94$ for $\Delta\alpha_{in} = +1.8^\circ$ and 0.92 for $\Delta\alpha_{in} = -2^\circ$.

Table 5.

Crystal	α/deg	L_e/mm $(+\Delta\alpha_{in})$	L_e/mm $(\Delta\alpha_{in}=0)$	L_e/mm $(-\Delta\alpha_{in})$	L_o/mm $(+\Delta\alpha_{in})$	L_o/mm $(\Delta\alpha_{in}=0)$	L_o/mm $(-\Delta\alpha_{in})$	μ/deg $(+\Delta\alpha_{in})$	μ/deg $(-\Delta\alpha_{in})$	ε/deg $(+\Delta\alpha_{in})$	ε/deg $(-\Delta\alpha_{in})$
$CaCO_3$	76.94	0	0.44	1.66	1.55	1.12	0	86.49	71.74	76.94	76.94
	60	**0**	**0.56**	**1.20**	**0**	**0.71**	**1.46**	**90.08**	**69.45**	**40.09**	**40.09**
α-BBO	76.9	0	0.61	1.71	1.64	1.04	0	87.68	71.67	76.90	76.90
	64.6	**0**	**0.59**	**1.31**	**0**	**0.71**	**1.52**	**89.47**	**70.20**	**50.78**	**50.78**
$LiIO_3$	**68.04**	**0.40**	**0.68**	**1.01**	**0.70**	**0.38**	**0**	**91.25**	**75.47**	**68.04**	**68.04**
	62.63	0	0.69	1.14	0	0.87	1.40	94.98	73.79	54.73	54.73
$LiNbO_3$	53.27	1.38	1.38	1.48	0.18	0.17	0.04	87.53	80.66	53.27	57.27
	65.38	**1.10**	**1.23**	**1.39**	**0.34**	**0.18**	**0**	**105.53**	**93.04**	**89.44**	**89.15**

Table 6.

Crystal	Prism type	α/deg	L_1/mm	L_2/mm	L_3/mm	H_1/mm	H_2/mm	H_3/mm	L_{in}/mm	d_e/d_{in} $(+\Delta\alpha_{in})$	d_e/d_{in} $(\Delta\alpha_{in}=0)$	d_e/d_{in} $(-\Delta\alpha_{in})$
YVO_4	III	**64**	**11.91**	**11.91**	–	**5.70**	**4.50**	–	**0**	**0.57**	**0.50**	**0.41**
	IV	61.6	22.02	20.52	10.92	9.21	6.82	0.81	0	0.62	0.51	0.42
TiO_2	III	**53.81**	**10.91**	**9.56**	–	**4.04**	**4.04**	–	**0**	**0.49**	**0.40**	**0.33**
	IV	45	27.45	23.48	8.78	7.25	7.25	1.42	1.1	0.49	0.40	0.33

Notes: $d_o/d_{in} = 1$ for all prisms; in TiO_2 IV prism for $L_{in} = 0$, the e-beam is vignetted on the Brewster face.

Table 7.

Crystal	α/deg	L_e/mm $(+\Delta\alpha_{in})$	L_e/mm $(\Delta\alpha_{in}=0)$	L_e/mm $(-\Delta\alpha_{in})$	L_o/mm $(+\Delta\alpha_{in})$	L_o/mm $(\Delta\alpha_{in}=0)$	L_o/mm $(-\Delta\alpha_{in})$	μ/deg $(+\Delta\alpha_{in})$	μ/deg $(-\Delta\alpha_{in})$	ε/deg $(+\Delta\alpha_{in})$	ε/deg $(-\Delta\alpha_{in})$
YVO_4	**64**	**1.06**	**1.22**	**1.38**	**0.44**	**0.22**	**0**	**89.82**	**75.88**	**64**	**64**
	61.6	0	0.42	0.68	0	0.59	0.95	91.08	74.18	56.77	56.77
TiO_2	**53.81**	**1.02**	**1.11**	**1.16**	**0.22**	**0.01**	**0**	**90.10**	**77.78**	**53.81**	**53.81**
	45	0.04	0.20	0.31	0	0.27	0.45	91.95	79.63	39.47	39.47

and α-BBO crystals are most convenient for fabricating most compact prisms IV.

The splitting of polarised beams by the method described above provides their separation by large angles even by using prisms made of crystals with a relatively small birefringence. For example, a small prism III made of the $LiNbO_3$ crystal (Tables 4 and 5) with the birefringence $\Delta n \approx 0.08$ separates the o- and e-beams by the angle $\mu = 87.4^\circ$ (Table 2). A considerable disadvantage of this prism is its relatively narrow and asymmetric field of view $\Delta\alpha_{in} = -2^\circ \ldots + 0.04^\circ$. Note that the width of the field of view of prism IV made of the same crystal is almost twice as large as that for prism III (Table 2). However, because the angle θ is 190.46°, it will be difficult to fabricate such a prism. This problem can be solved by abandoning the normal output of the o-wave and fabricating this prism IV as a trihedral prism (we denote it as prism IV → III) with the angles α and β corresponding to prism IV, but with other values of angles $\theta = 180^\circ$ and $\psi = \gamma = 37.92^\circ$. Upon the normal incidence of the input beam, the o-wave will come out from the ADM face of new IV → III prism at an angle of $\sim 24^\circ$ to the right (along the wave propagation) with respect to the normal. Because the reflection of this beam from the ADM face without the AR coating only weakly differs from reflection upon normal incidence (17 % vs 14.5 %), the interference AR coating of this face will be simple.

A comparison of the angles ε and μ shows that the rotation of the prism is accompanied by the rotation of the e-beam without a change in the angular position of the o-beam. Such a stability of the o-beam is caused by the even number of its reflections in the prism.

Upon the deviation of the incident beam from the normal, there exists the residual reflection of the e-wave from the Brewster face (the e-reflex), whose energy propagates along the o-wave. If the angle between the wave vectors of the e-reflex and the o-wave is too small, the polarisation extinction (the intensity ratio of orthogonally polarised light components) of the latter will drastically decrease. The behaviour of the e-reflex is described by the solutions of the corresponding Snell equations for reflection from the BC face and refraction on the DC face (AM in prisms III), which can be found as the solutions of Eqns (4) and (6). The solutions obtained in this way showed that the e-reflex always comes out from the prism with deviation to the right with respect to the wave vector of the o-wave. These deviation angles are different for different prisms, and lie in the range from 6.6° to 16.2° for the six optimal prisms (Table 8), varying only slightly within the field of view of the prisms. The latter means that any nonzero e-reflex in the far-field zone does not deteriorate the polarisation extinction of the beam because it 'swings' together with the beam at an almost constant distance from it.

Table 8.

Crystal	α/deg	Output angle of the e-reflex with respect to the o-beam/deg		
		$-\Delta\alpha_{in}$	$\Delta\alpha_{in} = 0$	$+\Delta\alpha_{in}$
$CaCO_3$	60	8.48	8.43	8.40
α-BBO	64.6	9.23	9.18	9.16
$LiIO_3$	68.04	6.65	7.71	6.78
$LiNbO_3$ (prism IV → III)	65.38	7.14	7.22	7.31
YVO_4	64	10.81	10.85	10.90
TiO_2	53.81	16.22	16.19	16.16

4. Thermal and dispersion properties of polarisation single prisms

We pointed out above that the deviation angle ε of the o-wave was stable upon prism rotation. Because of the crystal isotropy for the o-wave, this angle is also independent of the wavelength of light. However, it depends on temperature due to the thermal distortion of the anisotropic asymmetric prism.

As for the beam separation angle μ, because of the anisotropic reflection and refraction of the e-wave, it depends both on the wavelength of light and the prism temperature. Table 9 presents the temperature walk-offs $\Delta\mu$ and $\Delta\varepsilon$ of the angles μ and ε and the temperature shifts ΔL_o and ΔL_e of the beams at the output faces at the extreme points of the temperature range $T = 20 \pm 25\,^\circ C$ calculated for six optimal variants of prisms. The calculations were preformed for the normal incidence of the input beam by assuming that the thermal expansion coefficients $\alpha_\parallel$ (along the optical axis) and $\alpha_\perp$ (perpendicular to the optical axis) and the temperature derivatives dn_o/dT and dn_e/dT are constant in this temperature range. These parameters of the crystals, which are well known now [1, 5–9], are presented together with dispersion formulas for convenience in Table 10. Thermal variations in the prism shape were calculated within the theory of anisotropic expansion of crystals [5].

Table 9.

Crystal	α/deg	Δε/angular min	Δμ/angular min	ΔL_o/μm	ΔL_e/μm
$CaCO_3$	60	±2	±9	∓8	∓11
α-BBO	64.6	∓3	∓9	±11	±17
$LiIO_3$	68.04	0	±13	∓4	∓1
$LiNbO_3$ (prism IV → III	65.38	∓3	∓19	∓1	∓3
YVO_4	64	∓1	∓5	∓3	±4
TiO_2	53.81	0	∓1	∓1	±1

The calculations showed that the deviations $\Delta\mu$, $\Delta\varepsilon$, ΔL_o, and ΔL_e in our temperature range are almost linear functions vanishing at $\Delta T = 0$. One can see from Table 9 that the range of variations of the angle ε is several angular minutes, while that of the angle μ – from a few to two tens of minutes. Thermal walk-offs of the beams at faces are small and do not exceed ±17 μm in the worst case.

To design prisms in practice, aside from their thermal characteristics, it is also useful to know their dispersion properties. Consider the displacements of light beams on the output faces and changes in the beam separation angle μ for a prism operating at wavelengths other than the specified wavelength. Figures 5 and 6 present the calculated dispersion dependences of the relative changes in the position of the axis of the e-beam on its output face $[L_{e1}(\lambda) - L_{e1}(\lambda = 1.064\ \mu m)]/L_{e1}(\lambda = 1.064\ \mu m)$ and the separation angle for the o- and e-beams $[\mu(\lambda) - \mu(\lambda = 1.064\ \mu m)]/\mu(\lambda = 1.064\ \mu m)$ for optimal prisms for the normally incident input beam. The dispersion of the angle μ is the sum of dispersions of the angle of TIR of the e-wave from the AGD face (Fig. 1) and its angle of refraction on the output face BC. In some crystals, these dispersions can be almost completely compensated, for example, in a $CaCO_3$ prism IV (Fig. 6).

Table 10.

Crystal	Dispersion formulas of refraction coefficeints (λ in μm)	$dn_o/dT/10^{-6}\,^\circ C^{-1}$	$dn_e/dT/10^{-6}\,^\circ C^{-1}$	$\alpha_\parallel/10^{-6}\,^\circ C^{-1}$	$\alpha_\perp/10^{-6}\,^\circ C^{-1}$	References
$CaCO_3$	$n_o = [2.69705 + 0.0192064/(\lambda^2 - 0.0182) - 0.0151624\lambda^2]^{1/2}$ $n_e = [2.18438 + 0.0087309/(\lambda^2 - 0.01018) - 0.0024411\lambda^2]^{1/2}$	+2.08*	+1.85*	+25	−5.6	[1, 5–8]
α-BBO	$n_o = [2.7471 + 0.01878/(\lambda^2 - 0.01822) - 0.01354\lambda^2]^{1/2}$ $n_e = [2.3174 + 0.01224/(\lambda^2 - 0.01667) - 0.01516\lambda^2]^{1/2}$	−9.3	−16.6	+4	+36	[6]
$LiIO_3$	$n_o = [2.03132 + 1.37623\lambda^2/(\lambda^2 - 0.0350823) + 1.06745\lambda^2/(\lambda^2 - 169)]^{1/2}$ $n_e = [1.83086 + 1.08807\lambda^2/(\lambda^2 - 0.031381) + 0.554582\lambda^2/(\lambda^2 - 158.76)]^{1/2}$	−89.3	−75.2	+48	+28	[1, 9, 10]
$LiNbO_3$	$n_o = [2.39198 + 2.51118\lambda^2/(\lambda^2 - 0.217^2) + 7.1333\lambda^2/(\lambda^2 - 16.502^2)]^{1/2}$ $n_e = [2.32468 + 2.2565\lambda^2/(\lambda^2 - 0.21^2) + 14.503\lambda^2/(\lambda^2 - 25.915^2)]^{1/2}$	+5.4	+38	+4.1	+14.8	[1, 11]
YVO_4	$n_o = [3.77834 + 0.069736/(\lambda^2 - 0.04724) - 0.0108133\lambda^2]^{1/2}$ $n_e = [4.59905 + 0.110534/(\lambda^2 - 0.04813) - 0.0122676\lambda^2]^{1/2}$	+8.5	+3	+11.37	+4.43	[6]
TiO_2	$n_o = [5.913 + 0.2441/(\lambda^2 - 0.0803)]^{1/2}$ $n_e = [7.197 + 0.3332/(\lambda^2 - 0.0843)]^{1/2}$	−0.72	−0.42	+9.2	+7.14	[1]

* For $\lambda = 0.645$ μm. In [8], the values of dn_o/dT and dn_e/dT for $CaCO_3$ are presented only for the spectral range from 0.441 to 0.645 μm. These data show the decrease of the derivatives dn_o/dT and dn_e/dT with increasing the wavelength.

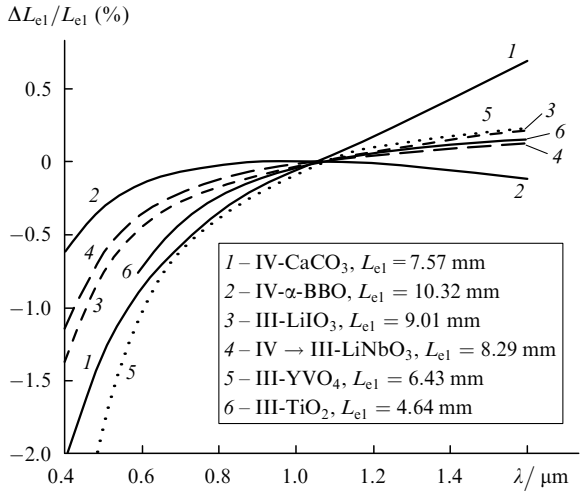

Figure 5. Dispersion dependences of displacements of the e-beam axes on Brewster faces of optimal prisms made of different crystals. The absolute displacement $\Delta L_{e1} = L_{e1}(\lambda) - L_{e1}(\lambda = 1.064\ \mu m)$ is normalised to the values of L_{e1}, which are different for different prisms ($\lambda = 1.064$ μm) and presented in the figure.

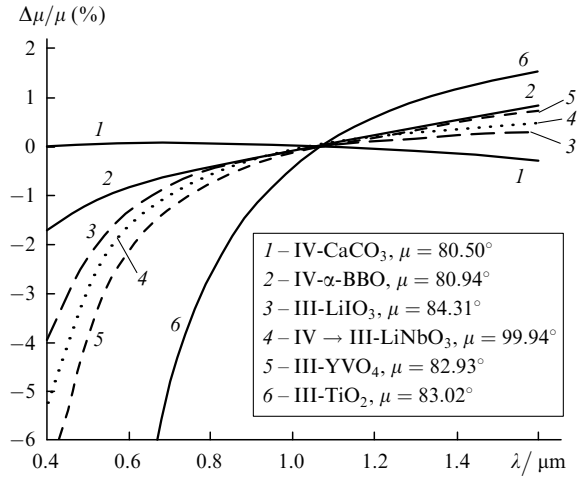

Figure 6. Dispersion dependences of the splitting angles of orthogonally polarised beams on the Brewster faces of optimal prisms made of different crystals. The absolute change in the splitting angle $\Delta\mu = \mu(\lambda) - \mu(\lambda = 1.064\ \mu m)$ is normalised to the values of $\mu(\lambda = 1.064\ \mu m)$, which are different for different prisms and are presented in the figure.

As for the o-beam, its dispersion behaviour is reduced only to small displacements on the output face, these displacements being manifested only when the input beam is incident on the AB face (Fig. 1) not strictly normally. The maximal displacements $\Delta L_o = |L_o(\lambda) - L_o(\lambda = 1.064\ \mu m)|$ (Fig. 4) take place in the short-wavelength part of the spectrum at the edges of the field of view. The greatest displacement $\Delta L_o \sim 19$ μm was observed for the α-BBO IV prism at $\alpha = 0.4$ μm.

The deviation angle ε in the $LiNbO_3$ IV → III prism weakly depends on the angle of incidence α (Table 5) and the wavelength because the angle of refraction of the output o-wave is 24°. The relative variations of this angle at the spectral boundaries of its wavelength dependence $\lambda = 0.4$ and 1.6 μm (for the normally incident input beam) are $\Delta\varepsilon/\varepsilon(\lambda = 1.064\ \mu m) = +2.6\,\%$ for $\lambda = 0.4$ μm and $-0.3\,\%$ for $\lambda = 1.6$ μm, where $\Delta\varepsilon = \varepsilon(\lambda) - \varepsilon(\lambda = 1.064\ \mu m)$.

The angular fields of view $\pm\Delta\alpha_{in}$ in all prisms, except the TiO_2 prism, narrow down with increasing the wavelength from the side of their 'positive' (+) boundaries. This is caused by the violation of TIR of the o-wave upon a dispersion decrease in the refraction coefficient n_o. On passing from $\lambda = 1.064$ μm to $\lambda = 1.6$ μm, these boundary values decrease from 4° to 3.5° in the $CaCO_3$ IV prism, from 3.5° to 3.1° in the α-BBO IV prism, from 2.6° to 2.3° in the $LiIO_3$ III prism, from 1.8° to 1.2° in the $LiNbO_3$ IV → III prism, and from 2.4° to 2.0° in the YVO_4 III prism. This effect is absent in rutile III prism because the angle of reflection of the o-wave from the BC face considerably exceeds the corresponding critical TIR angle.

5. Compensation of the anamorphism of the e-beam, spectral and temperature dependences of their separation angles of polarised beams

The obvious disadvantages of single-prism polarisation beamsplitters listed in this heading can be easily removed in beamsplitters consisting of symmetric combinations of basic prisms. Figure 7 shows two such combinations: one of them consists of two IV prisms and the other – of two III prisms (both combinations are shown conventionally in one common figure). It is important in this case that now both the o- and e-waves experience the even number of reflections. As a result, the e-beam comes out of the prism parallel to the input beam with the displacement S_{ray} specified by the condition that the positions of the beams on the input and output normal faces are the same. This displacement linearly depends on the gap d_{pr} between the prisms:

$$S_{ray} = k_1 d_{pr} + b_1. \quad (11)$$

The same condition that the positions of the beams are the same requires that the second prism should be displaced by S_{pr} with respect to the first prism:

$$S_{pr} = k_2 d_{pr} + b_2. \quad (12)$$

The constants k_1, k_2, b_1,nd b_2 for the prism intended for a beam of diameter 5 mm are presented in Table 11.

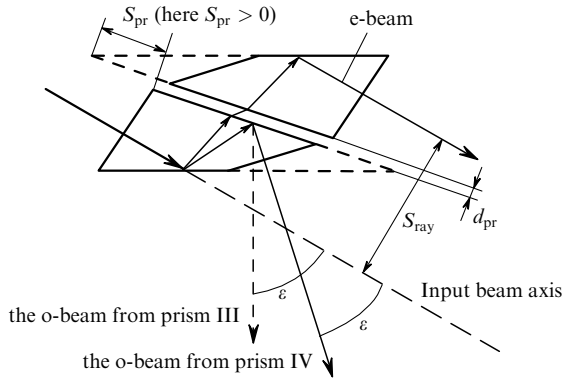

Figure 7. Thermally stable, dispersion-free, two-prism polarisation beamsplitter with Brewster refractions of the e-wave on the surfaces of the air gap, which is free of the astigmatism of both beams.

Table 11.

Combined two-prism beamsplitter	k_1	b_1/mm	k_2	b_2/mm
$CaCO_3$ (prisms IV)	1.279160	14.896950	−1.701149	6.705045
α-BBO (prisms IV)	1.000240	15.818980	−1.722201	1.248751
$LiIO_3$ (prisms III)	0.590000	7.709001	−1.854671	−4.357828
$LiNbO_3$ (prisms IV → III)	0.455471	7.231713	−2.250346	−4.949916
YVO_4 (prisms III)	0.769632	6.329463	−2.151470	−2.112102
TiO_2 (prisms III)	1.431937	6.319031	−2.758295	0.794684

Notes: The parameter d_{pr} is measured in mm by using the data from the table for calculations by expressions (11) and (12).

Beamsplitters in Fig. 7 split polarised beams by the angles coinciding with angles ε in the corresponding single prisms. The dispersion of the refractive indices is now manifested only in small variations in the displacement S_{ray} depending on the wavelength. But even these variations can be minimised by a proper selection of the gap d_{pr}. This is possible because S_{ray} also depends on the dispersion variations in the output angle α_{out} of the e-beam and its position L_{el} on the BC face (see Figs 1, 4). For large gaps, the influence of angular variations $\Delta\alpha_{out}$ dominates, while for small gaps, displacement variations ΔL_{el} are dominant. Figure 8 shows the wavelength dependences of relative variations $\Delta S_{ray}/S_{ray}(\lambda = 1.064\ \mu m)$ in the displacement minimised in the region $\lambda = 1.064$ μm. Note that the combination of calcite IV prisms cannot be minimised in this way [curves (*1*) and (*2*)]. This is explained by a weak dispersion of the output angle of the e-beam in this prism [curve (*1*) in Fig. 6].

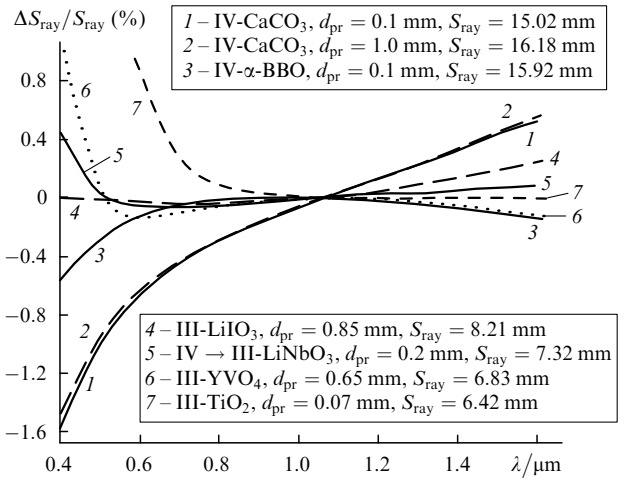

Figure 8. Dispersion dependences of displacements of e-beams with respect to the input beam for optimal prisms made of different crystals. The absolute displacement $\Delta S_{ray} = S_{ray}(\lambda) - S_{ray}(\lambda = 1.064\ \mu m)$ is normalised to the values of $S_{ray}(\lambda = 1.064\ \mu m)$, which are different for different prisms and are shown in the figure.

The thermal deviations $\Delta S_{ray} = [S_{ray}(T) - S_{ray}(T = 20\,^{\circ}C)]$ at the boundaries of the temperature range $T = 20 \pm 25\,^{\circ}C$ calculated for beamsplitters consisting of optimal single prisms are presented in Table 12. The values of ΔS_{ray} lie in the interval ∼ 25 μm in the 'worst' case (beamsplitter

Table 12.

Combined two-prism beamsplitter	$d_{pr} = 0.1$ mm		$d_{pr} = 1.0$ mm	
	S_{ray}/mm	ΔS_{ray}/μm	S_{ray}/mm	ΔS_{ray}/mμ
$CaCO_3$ (prisms IV)	15.02	∓1.6	16.18	∓4.8
α-BBO (prisms IV)	15.92	±9.1	16.82	±11.5
$LiIO_3$ (prisms III)	7.77	±9.3	8.30	0
$LiNbO_3$ (prisms IV → III)	7.28	±12.6	7.69	±8.1
YVO_4 (prisms III)	6.41	±4.5	7.10	±8.8
TiO_2 (prisms III)	6.46	±1.5	7.75	±3

Notes: Calculations are performed for radiation at 1.064 μm; $\Delta S_{ray} = [S_{ray}(T) - S_{ray}(T = 20^{\circ}C)]$; values of ΔS_{ray} and their signs correspond to temperature variation $\Delta T = \pm 25\,^{\circ}C$ relative to room temperature $+20\,^{\circ}C$.

consisting of $LiNbO_3$ prisms with $d_{pr} = 0.1$ mm). For other beamsplitters, these values are even smaller.

It is often important in practice that one of the beams at the output of a polarisation beamsplitter would be a continuation of the incident beam. Figure 9 shows how this can be realised in the simplest way. Here, the o-beam propagates with the help of prism No. 3, which is analogous to prisms Nos 1 and 2, in the same direction as the incident beam. In this case, all its positive properties are preserved. The angular adjustment of prism No. 3 in the propagation plane of the beams should not be very complicated due to the even number of reflections of the o-wave in each of the prisms. The coaxial alignment of the o-beam with the incident beam is mainly achieved with the help of translational displacements of this prism, which can be readily performed. Note that optical images transferred through both 'polarised' channels are not inverted in this triple combination.

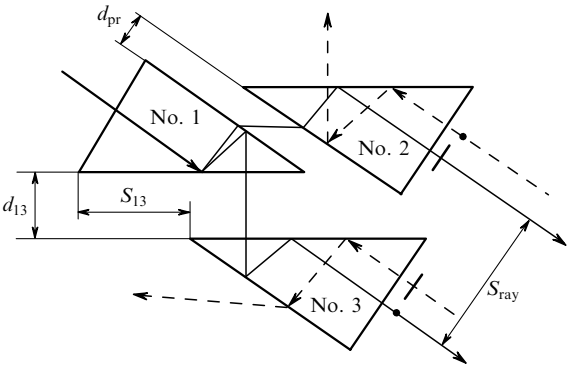

Figure 9. Thermally stable, dispersion-free, non-astigmatic polarisation beamsplitter assembled from prisms III, without the displacement of the o-beam from its initial direction and with the parallel output of both beams. The dashed straight lines show the propagation directions of counterpropagating beams with polarisation orthogonal to that of the forward beams.

Expressions for the calculation of the gap d_{13} and the corresponding displacement S_{13} (Fig. 9) for particular prisms can be derived using the beam propagation geometry. For example, for prisms III the expressions

$$S_{13} = 2(L_2 - L_o) - L_1 - d_o, \tag{13}$$

$$d_{13} = \frac{S_{13} + L_1}{\tan\alpha} - \frac{2L_1 + d_o}{\sin\alpha} \tag{14}$$

can be easily obtained. Here, the values of α, L_o, L_1, and L_2 for the corresponding crystals are taken from Tables 4–7, the value of L_o being taken from the column corresponding to $\Delta\alpha_{in} = 0$. The values of S_{13} and d_{13} obtained in this way will correspond to the combined beamsplitter with the light aperture 5 mm. Note that the displacement S_{ray} of the e-ray with respect to the o-ray in this combination of three single prisms is still specified by the gap d_{pr} according to (11).

In devices of the type of optical isolators and circulators, the ability of polarisation prisms to separate the forward and counterpropagating waves with orthogonal polarisations is used. The prisms described above are especially convenient for this purpose because they not only perform this operation with minimal reflection losses but also separate the beams by the angles of tens of degrees. The example of such a separation is shown in Fig. 9, where the propagation directions of counterpropagating orthogonally polarised waves are shown by the dashed lines.

As in the case of single prisms III, similar combined beamsplitters can be also composed from prisms IV. The longitudinal size of such beamsplitters (Fig. 10) can be reduced by using an auxiliary 45° glass rhomb.

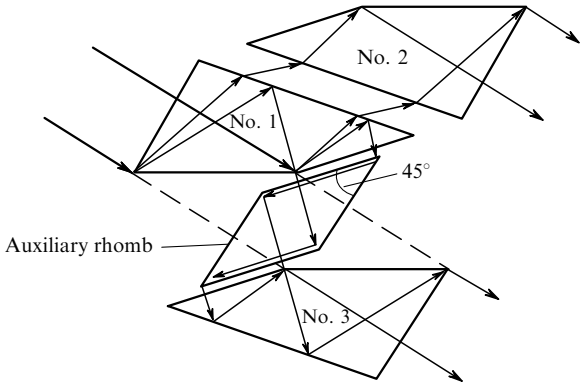

Figure 10. Thermally stable, dispersion-free, non-astigmatic polarisation beamsplitter assembled from prisms IV, without the displacement of the o-beam from its initial direction and with the parallel output of both beams. The longitudinal size of the beamsplitter is minimised by means of an auxiliary 45° glass rhomb.

As for prisms Nos 2 and 3, to compensate efficiently the temperature and dispersion walk-offs of the beams, these prisms irrespective of their type should be fabricated from the same material as prism No. 1. However, if small angular displacements of the o- and e-beams caused by temperature variations can be neglected, prisms Nos 2 and 3 can be made from glass. If the glass of prism No. 2 has the refractive index $n = \tan\alpha_{out}^{Br}$ (see Fig. 1), this can provide a technologically convenient parallelism of the gap. However, if in this case the output o- and e-beams should be parallel, the angular and linear dimensions of glass prism No. 2 will differ from those of prism No. 1. This is explained by different inner Brewster angles in the glass and crystal. If the parallelism of the beams is not required, the anamorphism of the e-beam coming out of prism No. 1 can be more conveniently corrected with the help of a usual glass wedge.

6. Experimental tests

To verify the correctness of our calculations, we performed experimental tests of calcite prisms IV fabricated for operation with light apertures of diameters 5 and 9 mm (Fig. 11). The prisms were projected for operation with Gaussian beams of diameters 2 and 4 mm (at the $1/e^2$ level) with the double margin in aperture. The prism angles were made with a tolerance $\pm 5'$. The optical axes were oriented in two orthogonal planes with a tolerance of $\pm 15'$. During the tests of individual single prisms and their combinations according to Fig. 7, we measured the output angles and polarisation extinctions of the beams. The error of angular measurements was ± 3 mrad. A light source was a diode-pumped, power-stabilised cw Yb^{3+} fibre laser ($\lambda = 1.064$ μm, $\Delta\lambda = 0.12$ nm, $P_{out} = 93$ mW). The laser emitted

a plane polarised Gaussian beam from the end of an anisotropic fibre with the numerical aperture NA = 0.1, which was collimated with replaceable two-lens objectives down to diameters 2 and 4 mm. The IR beams propagated through the polarisation beamsplitter were observed on the screen with the help of a Zenit NV-Ch visor with the angular resolution ~ 1 mrad. The azimuth of the polarisation plane with respect to the plane of incidence was controlled with a $\lambda/2$ plate.

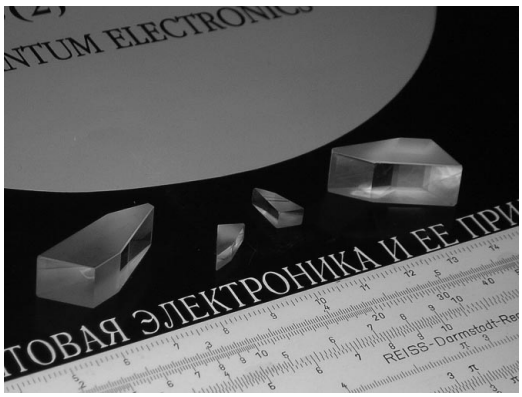

Figure 11. Photograph of calcite prisms IV with AR-coated normal faces fabricated for operation with light beams of diameters 5 and 9 mm. The scale division of a ruler is 1 mm.

The output angles of the o- and e-beams measured by the geometrical method in single prisms perfectly coincided within the above-mentioned errors with the angles presented in Table 2. In the two-prism combination (Fig. 7), the anamorphism of the e-beam was not observed visually in the far- and near field zones. The rotations of this combined beamsplitter as a whole within the angular field of view (and even more) do not change the propagation directions of the o- and e-beams.

The polarisation extinction was recorded with a precision Anritsu-ML9001A power meter and an analyser based on a standard Glan polariser with the rated extinction 52 dB. The extinctions of the beams measured in a single prism and a combined beamsplitter proved to be at least no less than the extinction of the polariser, i.e., no less than 52 dB.

7. Conclusions

Based on the study of the features of propagation of the e-wave in an optically anisotropic crystal, we have proposed the method for calculation and design of new crystal polarisers in the form of single prisms without gluing and gaps, which provide the splitting of polarised light beams by large angles with minimal reflection losses. The method ensures the conditions at which the e-wave leaves the prism at the Brewster angle to the output face, while the o-wave experiences TIR from the same face, coming out outside through another face normally to it.

The method has been illustrated by the characteristic variants of simple prisms made of six crystals, which are most often used in polarisation optics. Prisms close to optimal in their shape, size, and angular field of vision were determined for each of the crystals. The linear and angular parameters of the optimal prisms and their temperature and spectral dependences are presented in figures and tables in the convenient form.

It has been shown that the disadvantages of single prisms such as their anamorphism, the temperature and dispersion dependences of the angular and spatial positions of the output e-beam are eliminated in their glue-free symmetric combinations. In this case, by selecting properly the gap between prisms, the dispersion of the position of the e-beam on the output face can be minimised virtually in any spectral range.

New polarisation beamsplitters are compact and have a simple design. They can be applied in laser technologies using light beams with diameters up to ten millimetres.

References

1. Bass M., Van Stryland E.W., Williams D.R., Wolfe W.L. *Hand Book of Optics* (New York, San Francisco, Washington: R.R.Donnelly & Sons Comp., 1995) Vol. II.
2. Davydov B.L. *Single Crystal Polarizing Prism and Method of Manufacturing Thereof*. United States Patent No. US 6,690,514 B2 ; Feb.10 (2004).
3. Davydov B.L., Yagodkin D.I. *Kvantovaya Elektron.*, **35**, 1064 (2005) [*Quantum Electron.*, **35**, 1064 (2005).
4. Fedorov F.I. *Optika anizotropnykh sred* (Optics of Anisotropic Media) (Moscow: URSS, 2004).
5. Nye J.F. *Physical Properties of Crystals: Their Representation by Tensors and Matrices* (Oxford: Clarendon Press, 1957: Moscow: Mir, 1967].
6. www.casix.com.
7. www.adphotonics.com.
8. Abil'siitov G.A. (Ed.) *Tekhnologicheskie lazery (spravochnik), tom 2* (Handbook on Technological Lasers, Vol. 2) (Moscow: Mashinostroenie, 1991).
9. Gettemy D.J., Harker W.C., Lindholm G.L., Barnes N.P. *IEEE J. Quantum Electron.*, **24** (11), 2231 (1988).
10. Webb M.S., Velsko S.P. *IEEE J. Quantum Electron.*, **26** (8), 1394 (1990).
11. Zernike F., Midwinter J.E. *Applied Nonlinear Optics: Basics and Applications* (New York: Wiley, 1973; Moscow: Mir, 1976).